Supplementary Information for:

Programming an *in vitro* DNA oscillator using a molecular networking strategy

Kevin Montagne[1], Raphael Plasson[2], Yasuyuki Sakai[1], Teruo Fujii[1] & Yannick Rondelez[1]

This supplementary material contains:

Table SI: DNA oligonucleotides of the Oligator

T_1	A*A*CA**G*ACTC*GA-*AACA*GACT*C**GA-3'P
T_2	G*C*AT**GACTC**AT-AACA**GACTC**GA-3'P
T_3	T*T*ACTCGAAACAGACT-GCAT**GACTC**AT-3'P
α	TC**GAGTC**TGTT
β	AT**GAGTC**ATGC
Inh	*AGTCTGTTTCGAGT*AA

All sequences are given 5' to 3'. * indicates a phosphorothioate modification; 3'P indicates a 3' terminal phosphate modification used to block elongation; bold letters correspond to the nicking enzyme Nt.BstNBI recognition sequence. Italicized letters on T_1 and Inh indicate their matching subsequences. Note that only T_1, T_2, T_3 and α are necessary to start the oscillatory system.

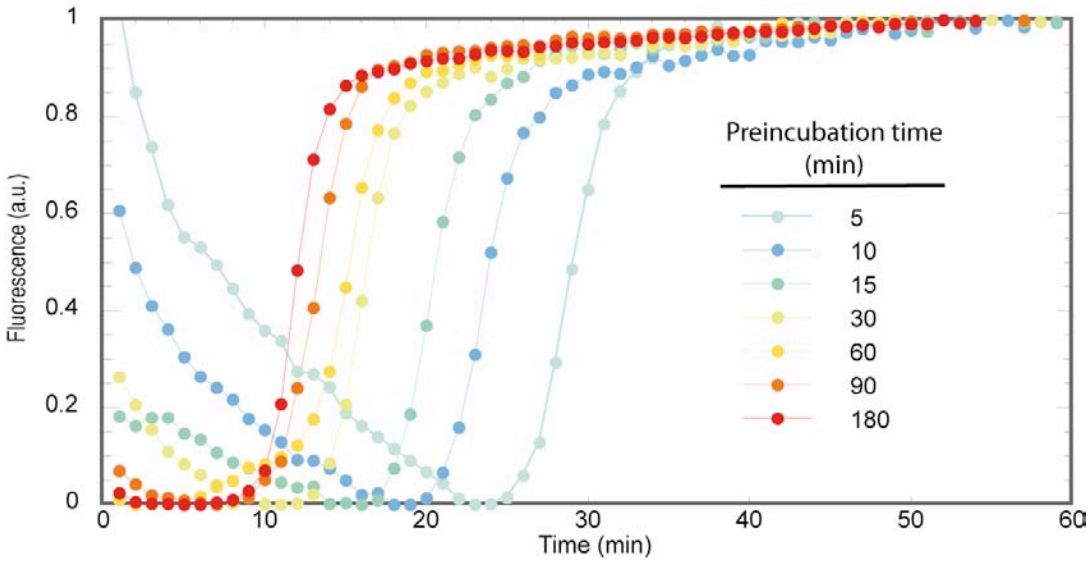

Figure S1: Release of the inhibition of T_1 by Inh in the presence of RecJ. T_1 (60nM) and Inh (60nM) were annealed in the reaction buffer and RecJ (30unit.mL^{-1}) was introduced. This mixture was incubated at 38.5ºC for various preincubation times, after which (at t=0) Bst (16 unit.mL^{-1}), NBI (200 unit.mL^{-1}) and α (0.1nM) were introduced to start the amplification reaction.

Supplementary text S1. Thermodynamic and kinetic constants for oligonucleotide hybridization.

Thermodynamic parameters for the binding of α to T_2, β to T_3, Inh to T_1 and Inh to T_3 were obtained from absorbance melt curves recorded at 260 nM in buffer A. Each oligomer was at a concentration of 1.43 μM.

The raw values were treated as described (Mergny and Lacroix, 2002) in order to yield the dissociated fraction θ for each temperature. We obtained the thermodynamic parameters from a linear regression of the plot of $\ln(K_a) = \theta / (1-\theta)$ versus 1/T.

The resulting thermodynamic parameters are shown in Table SII. We calculated the association constant at 38.5°C and compared it to the values estimated by the nearest-neighbour method and parameters. All of our values are somewhat smaller, which can be attributed to the presence of trehalose in the buffer (Spiess *et al*, 2004).

The association kinetic constants were evaluated using temperature-jump experiments (Nelson and Tinoco, 1982) in pseudo-first order conditions. α, β and Inh were mixed with templates in a 10 to 1 ratio so that their concentrations could be considered constant. By neglecting the backward dissociation, the reaction considered comes down to:

$$\text{oligomer} + \text{template} \longrightarrow \text{oligomer.template}$$

which is associated with a large fluorescent shift in the presence of EvaGreen. The apparent first order rate V then follows $V = k_{app}.[\text{template}]$, where $k_{app} = k_a.[\text{oligomer}]_0$, whith $[\text{oligomer}]_0$ being the total concentration of oligomer in the reaction and k_a the second order kinetic constant.

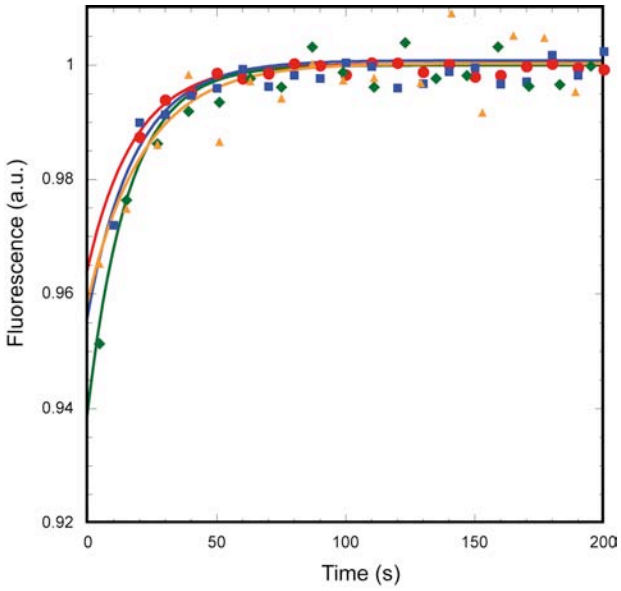

Figure S2. Kinetics of oligonucleotide hybridization. Oligomers (α, β or Inh) at 125 nM and the corresponding templates (T_2, T_3 or T_1) at 12.5 nM were mixed in buffer A in the presence of EvaGreen. The mixture was quickly brought from 70 to 38.5ºC and the fluorescence recorded. Orange triangles: β/T3; blue squares: α/T2; red dots: inh/T1; green diamonds: inh/T3; in each case, the solid line of matching colour is the best fit to $y = A(1-Be^{-kt})$.

The fluorescence is then given by the relation $F = F_0(1-e^{-k_{app}.t})$. The parameters obtained from the fit in Fig. S1 are given in Table SII. These values are well within typical short oligonucleotide kinetic association constants (between 10^5 and 10^6 $M^{-1}s^{-1}$; Zhang and Winfree, 2009). As they are, as expected, very similar, an average was calculated and used for the model.

Table SII: thermodynamic and kinetic parameters for hybridization reactions.

	ΔH measured (kcal.mol^{-1})	ΔS measured (cal.mol^{-1}.T^{-1})	K_a(38.5°C) (10^7M^{-1})	k_a (10^7M^{-1}.min^{-1})	$k_d = \frac{k_a}{K_a}$ (min^{-1})	K_a(38.5°C) predicted† (10^7M^{-1})
α/T_2	-94.9	-272	1.1 ± 0.3	3.0 ± 0.6	2.3 ± 0.7	6.7
β/T_3	-71.3	-197.1	2.7 ± 0.4	2.2 ± 0.7	.81 ± 0.4	6.8
Inh/T_1	-116.5	-329.6	450 ± 100	2.6 ± 0.6	0.0057 ± 0.002	2640
Inh/T_3	-122.3	-346.5	1200 ± 300	2.6 ± 0.6	0.0021 ± 0.001	6680
Average	NA	NA	NA	2.6 ± 0.6	NA	NA

All error bars are 1 s. d. formal errors calculated from least-square fitting and concentration measurement uncertainties. †Calculated using Dinamelt (Markham and Zuker, 2005)) and salt conditions of buffer A.

Supplementary text S2. Enzyme kinetic parameters

We measured the parameters of Michaelis-Menten kinetics ($V = k_{cat}.[S] / (K_m + [S])$, where [S] is the substrate's concentration, K_m and k_{cat} the Michaelis constant and rate, respectively) for all enzymatic reactions, using the fluorescent signal produced by oligonucleotides in the presence of EvaGreen. EvaGreen is a double-strand specific fluorescent intercalator; however the fluorescence induced by single-strand oligonucleotides (roughly 10 times lower; Mao *et al*. 2007) is sufficient to monitor variations in their concentrations. We took advantage of this feature to design reliable continuous assays to obtain k_{cat} and K_m for all enzymes. These experiments were conducted in the same conditions and temperature (38.5°C) used for oscillations. In each case, we checked whether or not the kinetic parameters were significantly different for the various substrates of the enzymes.

Bst DNA polymerase, Large Fragment, kinetic parameters

We measured the initial reaction rates for the polymerization of primer-template substrates $\alpha.T_2$ and $\beta.T_3$ (Template T_1 was not used to avoid the complications associated with the possibility for α to bind at two positions on T_1). This was done (Fig. S2) by following the fluorescence increase associated with the formation of template duplexes during the reaction:

$$\alpha.T_2 \xrightarrow{k_{pol}} T_{2duplex}$$

Bst polymerase can also recognize and elongate nicked substrates. In this case (strand displacing conditions), the reaction is expected to be slower because the enzyme needs to unwind the forward strand before it can add a new nucleotide to the nascent strand.

In the case of the nicked duplex $\beta.T_3.Inh$, the corresponding reaction:

$$\beta.T_3.Inh \xrightarrow{k_{pol,SD}} T_{3duplex} + Inh$$

does not produce a strong change in the fluorescent signal. Therefore we designed a multiple turnover assay to measure the continuous accumulation of Inh during the reaction:

$$\beta.T_3.Inh \xrightarrow{k_{pol,SD}} \xrightarrow{k_{Nick}} \beta.T_3.Inh + Inh$$

In the presence of excess nicking enzyme, the observed rate corresponds to the Inh-displacing rate for polymerization by *Bst*.

k_{cat} and K_m values are given in Table SIII. We also calculated k_{1st} which corresponds to the first order approximation, valid for substrate concentrations below the K_m. The K_m values were found within the large range of values reported for various polymerases (Kong *et al*, 1993)), and their location at the upper end of this range (for reactions without strand-displacement) might be linked to the short length of the primer and/or to the temperature of the assay which is much lower than the optimum for this enzyme (65ºC).

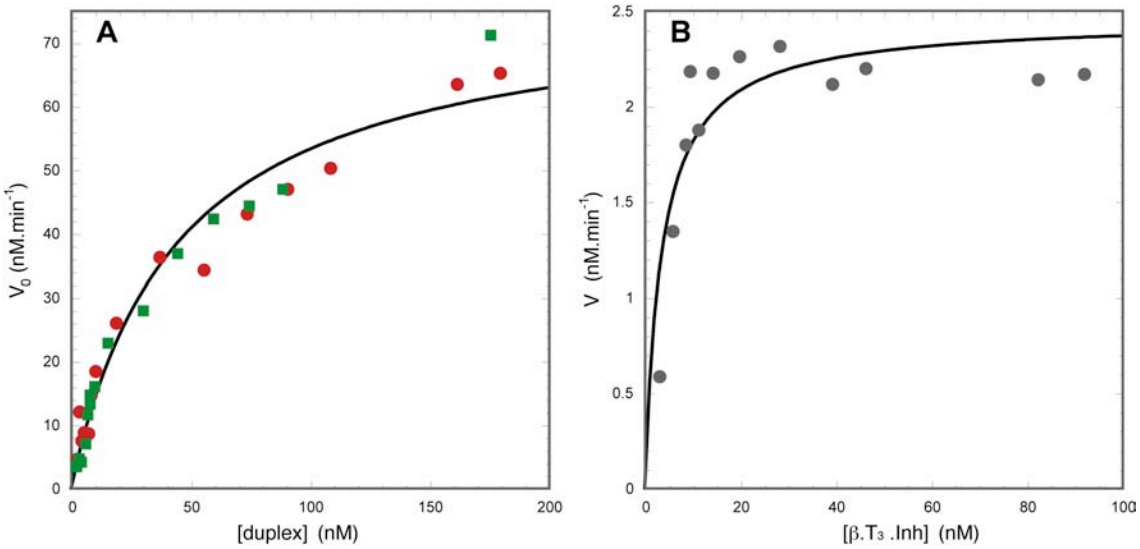

Figure S3. Kinetics of *Bst* polymerase. (**A**) Polymerization in the absence of strand displacement. A mixture of α (respectively β) at 1μM was equilibrated at 38.5°C with various concentrations of T_2 (respectively T_3) from 2 to 192 nM. At time t = 0, we introduced the polymerase (1.6 unit.mL^{-1}) and followed the fluorescence increase associated with the elongation of the primer-template complex. The initial reaction rate was plotted versus the concentration of primer-template substrates (calculated using oligonucleotide concentration and the previously determined binding constants). Green squares: $\alpha.T_2 \longrightarrow \alpha\beta.T_2$; red circles: $\beta.T_3 \longrightarrow \beta Inh.T_3$. Considering the experimental errors, no significant difference was observed for the two substrates, so all the points were used together to extract the Michaelis-Menten kinetic parameters (solid line). (**B**) Polymerization with strand displacement. A mixture containing Inh (500 nM), β (500 nM) and T_3 at various concentrations from 3 to 100 nM was incubated at 38.5°C in the presence of *Bst* polymerase (1.6 unit.mL^{-1}) and excess Nt.bstNBI (5 unit.mL^{-1}). The large amount of Inh insured that the only possible substrate for the polymerase was $\beta.T_3$.Inh. We observed a steady fluorescent increase due to the accumulation of single strand Inh as the polymerase repeatedly extends its substrate. This increase rate is plotted here versus $\beta.T_3$.Inh concentration, calculated from β, T_3 and Inh concentrations using the binding constants (T_3 duplex is neglected). The solid line shows the best fit to the Michaelis-Menten equation.

Nt.BstNBI nicking endonuclease constants

Nt.BstNBI parameters were measured for T_1 and T_2 duplexes. When nicked, these duplexes partly dissociate into template, input and output oligonucleotides. We found it convenient to add excess $RecJ_f$ exonuclease so that unprotected oligonucleotides α or β were quickly digested. This simplifies the analysis by removing the fluorescent contribution of partial duplexes. In these conditions the rate-limiting step is the nicking event, while the global reaction is:

$$T_{1duplex} \longrightarrow T_1$$

This reaction is associated with a large fluorescent shift. Kinetic parameters were determined by plotting the observed rates versus duplex concentration and fitting to the Michaelis–Menten equation. The experimental results are shown in Fig. S3 and the parameters k_{cat}, K_m and k_{1st} are summarized in Table SIII. k_{1st} values for the two substrates were similar considering experimental errors, so an average value was calculated and used thereafter.

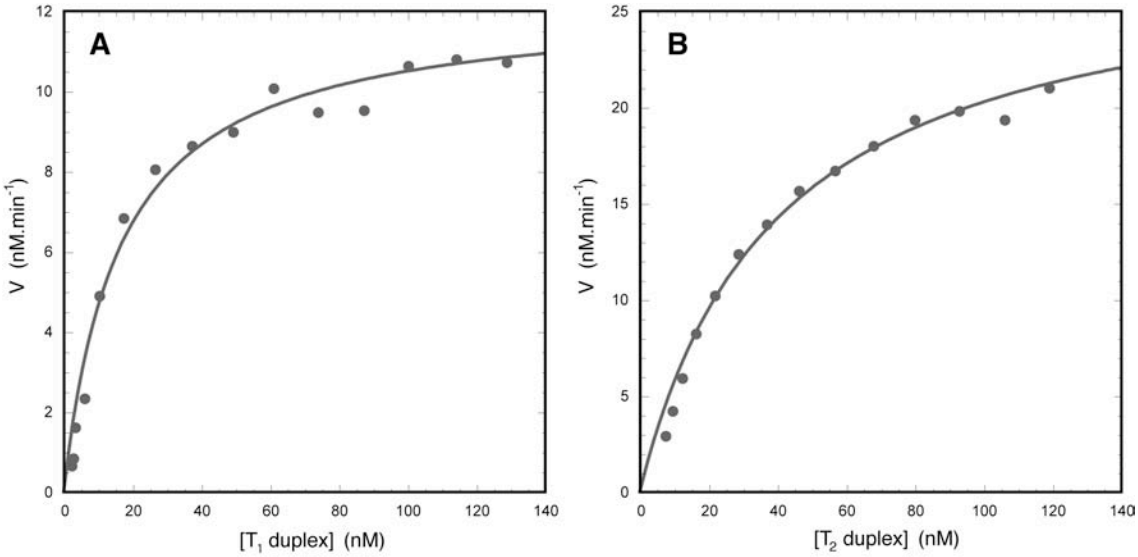

Figure S4. Kinetics of Nt.bstNBI nicking endonuclease. The fluorescence decrease associated to the nicking of substrates and subsequent digestion was measured for various duplex concentrations in buffer A + EvaGreen in the presence of 0.05 unit.μL^{-1} Nt.BstNBI and 1.5 unit.μL^{-1} RecJ$_f$. The nicking rates were calculated from this signal and plotted versus duplex concentrations. (**A**), nicking of $\alpha\alpha$.T$_1$; (**B**) nicking of $\alpha\beta$.T$_2$. The solid line is the best fit to the Michaelis-Menten equation.

RecJ$_f$ parameters

RecJ$_f$ (Lovett and Kolodner, 1989) is a non-thermophilic enzyme that quickly loses activity when used above 37°C. However, we found that trehalose at 400 mM efficiently stabilizes the enzyme at temperatures up to 42°C (data not shown).

The kinetic parameters were measured at 38.5°C by monitoring the fluorescent decrease due to the hydrolysis reaction of single-stranded substrates. The experimental points were directly used to fit the integrated Michaelis-Menten equation:

$$k_{cat}.t = S_0 - S(t) + K_m \ln(\frac{S_0}{S(t)})$$

where S(t) is the substrate concentration and S$_0$ the initial concentration, yielding the parameters listed in Table SIII. We applied the same assay to template T$_1$, which is protected by phosphorothioate bonds (Stein *et al,* 1988) and found a maximum hydrolysis rate $k_{cat}^{T_1}$ = 0.44 nM.min^{-1}, approximately 300 times slower than k_{cat}^{Inh}.

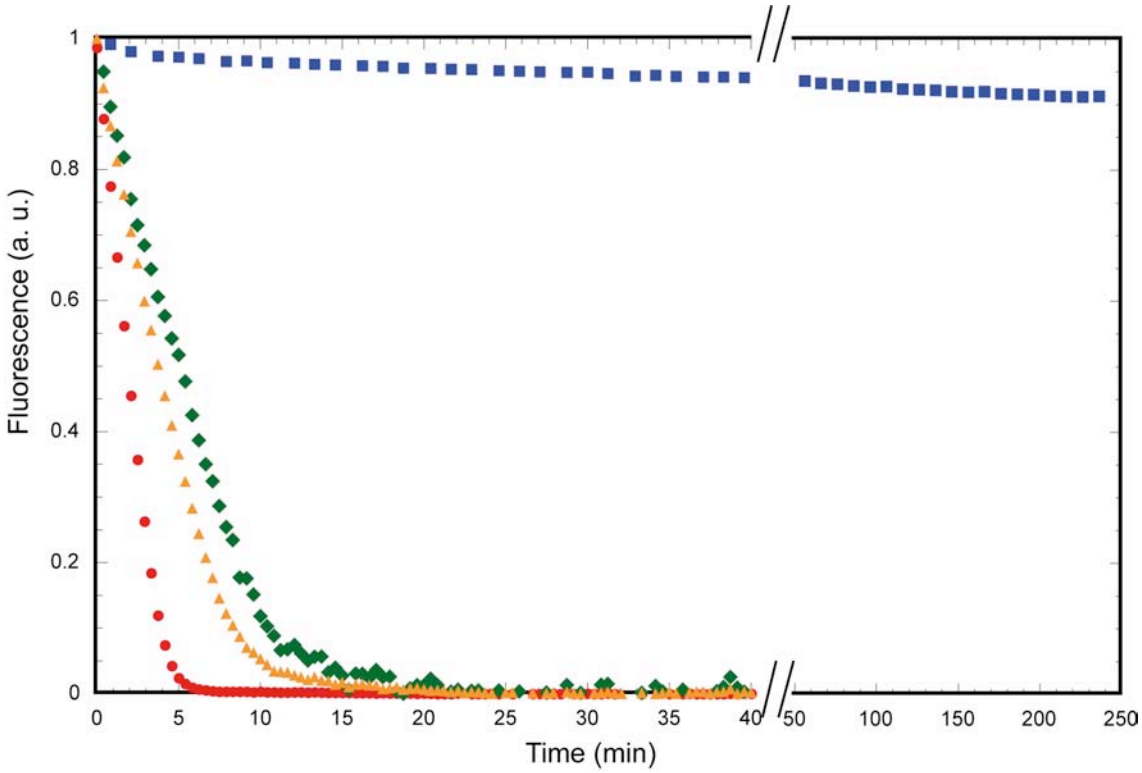

Figure S5. Kinetics of the hydrolysis of oligonucleotides by $RecJ_f$. The oligonucleotides (500 nM for Inh and T_1 and 1000 nM for α and β) were introduced in a mixture containing $RecJ_f$ at 0.045 unit/μL in buffer A + EvaGreen at 38.5°C. The fluorescence was recorded over time. Blue squares: T_1; red circles: Inh; green diamonds: α. yellow triangles: β. These curves were directly used to fit the integrated form of the Michaelis-Menten equation (not shown).

Table SIII: Michaelis-Menten and first-order parameters for enzymatic reactions

Enzyme	Substrate	k_{cat} (nM.min^{-1})	K_m (nM)	$k_{1st} = \frac{k_{cat}}{K_m}$ (min^{-1})	k_{1st} calculated for oscillator concentrations (min^{-1})
Nt.BstNBI 50 unit.μL^{-1}	T_1 duplex	12	15	0.80 ± 0.3	3.0 ± 1
	T_2 duplex	28	39	0.72 ± 0.2	
$RecJ_f$ 45 unit.mL^{-1}	α	140	305	0.48 ± 0.2	0.32 ± 0.15
	β	202	357	0.56 ± 0.2	0.37 ± 0.15
	Inh	168	92	1.8 ± 0.4	1.2 ± 0.3
Bst DNA polymerase 1.6 unit.mL^{-1}	α.T_2 β.T_3	77	44	1.7 ± 0.4	17 ± 4
	β.T_3.Inh (strand displacement)	2.4	3.5	0.69 ± 0.3	6.9 ± 3

All error bars are 1 s. d. formal errors calculated from least-square fitting and concentration measurement uncertainties.

Supplementary text S3. Measurement of the individual concentrations of α, β and Inh during the course of oscillations

In order to follow the evolution of [α], [β] and [Inh] during oscillations, we ran the oscillating reaction (20 µL) in the presence of radiolabeled ^{32}P dCTP. Aliquots were taken from the reaction at various time intervals starting from 120 minutes, immediately quenched by adding EDTA to a final concentration of 50 mM and stored at -20°C. 0.5 µL of these aliquots were dissolved in 4.5 µl of loading buffer and these samples were analyzed by 7M urea PAGE (Figure S6) and imaged with a Fujifilm phosphorimager during one night. The 16-mer and 11-mer band intensities were quantified using the software ImageJ (http://rsbweb.nih.gov/ij/): for each lane, we measured the average pixel intensity in an ellipse centred on the corresponding band and subtracted from this value the average intensity in the same ellipse positioned just above the band.

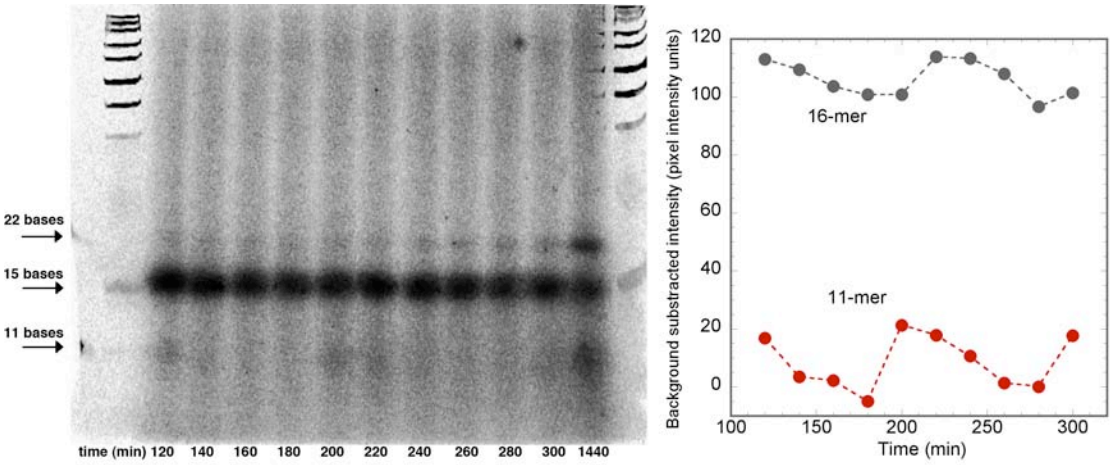

Figure S6. Radiolabeled gel analysis of the oscillating reaction. Left: autoradiogram of the denaturing gel. the outer lanes, corresponding to the size ladder, have been stained with SybrGreenII and their image superimposed on the autoradiogram. Numbers below each lane mark the reaction times in minutes. Right: quantification of the 16-mer and 11-mer band showing a cyclic accumulation of product in each case.

The gel clearly shows the band of a 16-mer product (attributed to Inh), and a faint accumulation of 11-mer products (attributed to α and β) can be detected in lanes separated by approximately 100 minutes. From Fig 2B (or from Fig S12) one expects Inh to oscillate between approximately 65 and 80nM (less than 20% variation), and therefore dark bands with a low amplitude variation should be observed. In contrast, (α + β) oscillate between almost zero and a total of approximately 20 nM. This is consistent with that fact that the 11-mer band intensity on the gel is approximately 4 times lower than the 16-mer band (all species contain two C bases, which is the labeled triphosphate used here) and that it goes down to background level.

The faint band at 22 bases can tentatively be attributed to elongated oligonucleotides that have not been nicked yet. No other significant product accumulation is detected until the end of the reaction (lane at 1440 minutes), suggesting that unexpected species don't accumulate, at least during the first oscillations.

However this gel analysis was not sensitive enough for quantitative analysis, so we used another technique to precisely quantify the concentrations of α, β and Inh.

Isothermal amplification reactions like the one shown in Fig. 1A of the main text can be used to find out the initial concentrations of trigger oligonucleotides in a process very similar to real time PCR (Van Ness *et al*, 2003). Indeed, the initial concentration of the trigger determines the moment when the fluorescent signal crosses a given threshold, and can be estimated by comparison with standard curves.

The oscillating reaction was reproduced again and aliquots were taken from the oscillating reaction at various time intervals, immediately quenched by adding EDTA to a final concentration of 20 mM and stored at -20°C. This sampling was started at t=235 min, after the system had approximately stabilized on its limit cycle. We conducted these assays in 45 mM Tris HCl, 50 mM NaCl, 10 mM KCl, 10 mM $(NH_4)SO_4$, 7 mM $MgCl_2$, 1 mM DTT, 0.1 % Triton X-100, pH=8.0, 1x EvaGreen (Biotium), 50 μM each dNTP (except for a lower amount of dNTP, this buffer is the one originally reported for the amplification reaction), in the presence of *Bst* DNA polymerase, Nt.BstNBI nicking endonuclease, and a template (60 nM) that contains a dual repeat of the analyte's complementary sequence.

α, β and Inh are present in the oscillating medium as a mixture of both single stranded and hybridized species. However, for α and β, the temperature at which we have conducted the remeasurement assay is very close to the melting temperature of these duplexes, so equilibration with assay templates is fast and we measure directly the total concentration of these species. In the case of Inh, where assay temperature is below the melting temperature of Inh/T_3, we have introduced a preheating step (65ºC, 2 min) to allow the mixture to equilibrate. One should note that in the remeasurement assay mixture the concentration of templates coming from the oscillating mix is always negligible compared to endogeneous assay templates (0.15nM vs 60nM).

We designed a specific assay for each target sequence (α, β and Inh) and carefully optimized the dynamic range in each case by changing the temperature and the concentration of both polymerase and nicking enzyme. These conditions are summarized in Table S4.

Quenched aliquots from the oscillating reaction were then diluted and 2 μL were introduced in PCR tubes containing 18 μL of the reaction mix. Reactions were done in triplicate. Standard dilution series were assembled at the same time, with all buffer and enzyme concentrations adjusted to match that of the unknown samples. These plates were then incubated at the indicated constant temperature in an iQ5 (BIORAD) real-time thermocycler, recording the fluorescence every 10, 15 or 6 seconds respectively for α, β and Inh. Analysis of the amplification curves and calculation of the target's initial concentration was performed using the built-in software.

Table SIV: Assay conditions for the determination of oligomer concentrations by quantitative isothermal amplification

Assay for :	α	β	Inh
Bst	2.5 unit.mL^{-1}	9.0 unit.mL^{-1}	3.0 unit.mL^{-1}
Nt.BstNBI	100 unit.mL^{-1}	100 unit.mL^{-1}	200 unit.mL^{-1}
Template sequence[a]	T_1 = AACA**GACTC**GAAAC A**GACTC**GA	T_β = GCAT**GACTC**ATGCA T**GACTC**AT	T_{Inh} = TTACTCGAAACAGA CTATAT**GACTC**TTAC TCGAAACAGACT
Temperature	39°C	39°C	46.7°C

[a] All sequences are given 5' to 3'; bold letters correspond to the nicking enzyme Nt.BstNBI recognition sequence.

Specificity and dynamic range of this kind of assay has been thoroughly investigated (Tan *et al*. 2008). However, to remove any concern about these points in our specific case, we also ran a control experiment in which various known concentrations of an analyte (e.g. β) were assessed with or without the presence of excess 'contaminant' (e.g. α). As an example, Fig S5 shows the influence of contaminant α on the detection of β: up to at least a 200 to 1 contamination ratio, no influence can be detected. Thus erroneous cross-detections can be ruled out. A similar result was obtained in the reverse case (no effect of excess β on the detection of α)

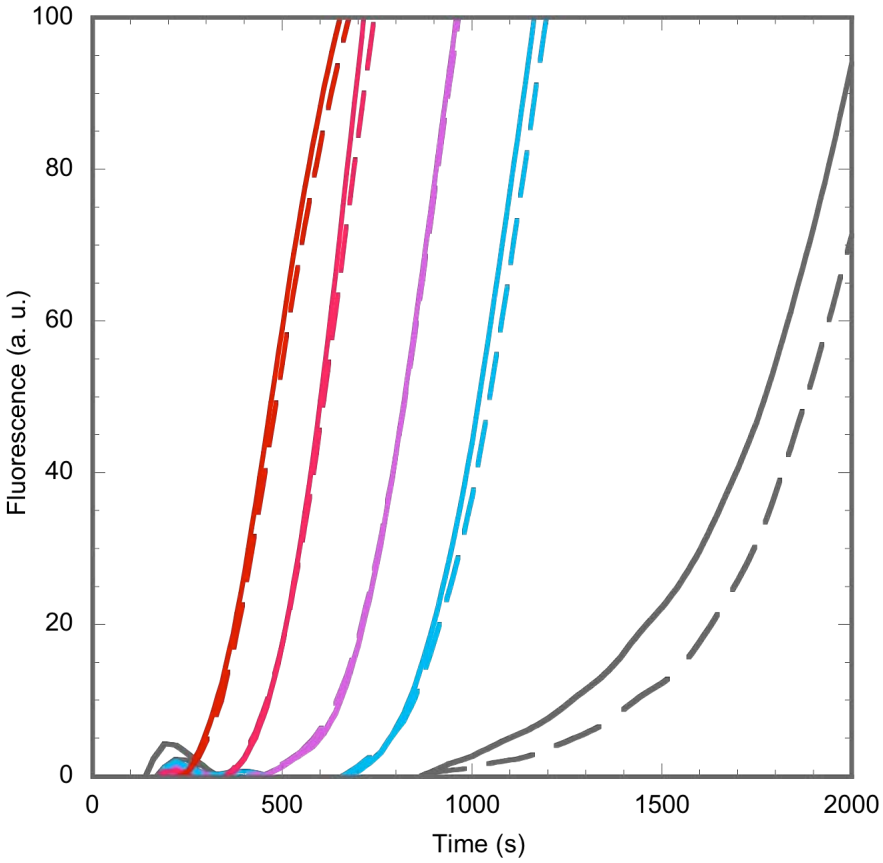

Figure S7. Isothermal amplification of β in the presence or absence of excess α. Various initial concentrations of β (red: 1250 pM; pink: 250 pM; purple: 50 pM; blue: 10 pM) were incubated in the assay conditions for β (Table SIV) with (dashed line) or without (full line) 5 nM α.

Supplementary text S4. Long-term evolution of the oscillations

During long oscillating experiments, the amplitude gradually decreases and a global slow exponential increase emerges in some cases (Fig. S6). We can propose one or a combination of the following factors to be responsible for these observations:

- Decrease in dNTP concentration (calculated from the model, in the conditions of Fig. 1C, each oscillation consumes roughly 3% of the initial concentration of dNTP,
- Accumulation of pyrophosphates (13 μM per cycle) that can have a deleterious effect on polymerization (Kramer and Coen, 2001),
- Decay of templates. Fig. S5 shows that protected templates, while much more stable than dynamic species, still decay in the presence of $RecJ_f$. As shown in Fig. 3 of the main text, changes in template concentrations may lead to drastic changes in the system's behaviour. For example, the decay of T_2 (present at an initially lower concentration) can ultimately lead to a disruption of the negative feedback loop. In this case, α would accumulate freely, because it cannot trigger the production of its inhibitor any more.
- Apparition of parasitic species. The emergence of self-amplifying parasites has been documented in a similar polymerase/nickase system (Tan *et al*, 2008),
- Accumulation of polymerization errors. Products containing errors can act as "poison", sequestering the templates,
- Loss of activity of the enzymes, especially $RecJ_f$, which is not thermostable.

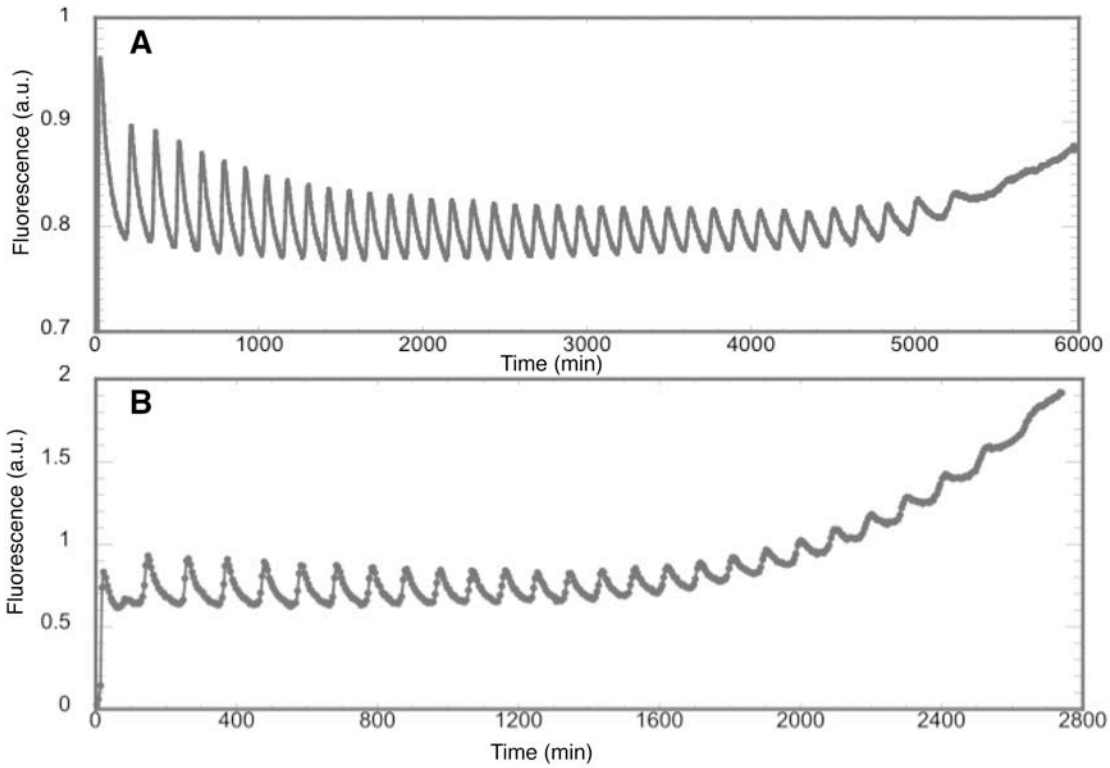

Figure S8. Long-term evolution of the oscillating systems. Typical time course of the fluorescent signal: (**A**) $[T_1]$ = 60 nM, $[T_2]$ = 5nM, $[T_3]$ = 90 nM. (**B**) $[T_1] = [T_3]$ = 30 nM, $[T_2]$ = 5nM (same experiment as Fig. 1C of the main text).

Supplementary text S5. Mathematical model

Chemical Network

The chemical network chosen to model the experimental system was as realistic as possible. The detail of all the reactions and their corresponding kinetic rates is given in Fig. S7. Several assumptions were made for the sake of simplicity:

- Because *Bst* polymerase and $RecJ_f$ are processive (Riggs *et al*, 1996; Han *et al*, 2006) enzymes, no intermediate species (partially polymerized or partially degraded strands) were taken into account,

- The decay of the templates was neglected (the maximum speed for hydrolysis of single strand templates is 300 slower than for unprotected strands; moreover in the course of the oscillating reaction, the templates spend a significant portion of their time in a double stranded state which is not recognized as a substrate by $RecJ_f$),

- Other possible non-ideal behaviours (loss of activity of the enzymes, phototoxicity or photobleaching resulting from repeated fluorescence recording…) were also neglected,

- First order kinetics was assumed for all enzymatic reactions. All measured concentrations for α , β and Inh (Fig. 2B of the main text) correspond to maximum substrate concentrations below the K_m for the three enzymes. This could also be verified afterwards, by checking the computed concentrations of all enzyme substrates. They were all indeed well below the corresponding K_m, except in one case: the production of Inh by polymerization with strand-displacement has a measured K_m of only 3.5 nM, while $\beta.T_3$.Inh maximal concentration was computed at 3.2 nM. It was assumed here that this deviation from linearity would be of small influence on the system, but this borderline assumption will be checked in future work,

- Kinetic and thermodynamic values for α, β and Inh were assumed to be independent of the template to which they bind. For example, the same k_a and K_a were assumed for the formation of $T_2.\beta$ or $\beta.T_3$.

A first calculation was performed directly with a limited number of kinetic parameters (Table 1) obtained in independent experiments (Supplementary text S2 and S3). This 'raw model' implies the further assumptions:

- The polymerization of $\alpha.T_1$ and $\alpha.T_2$ was supposed to occur at the same speed whether the output strand was binding the template (strand displacement) or not: because output α or β (located on the output side of the templates) are very close to their melting temperature, we expect that they dissociate early during the polymerisation process and thus marginally affect the rate. This assumption seems reasonable since Inh, which binds 3 orders of magnitude stronger than α or β only slows down the polymerization rate by a factor of 2.5,

- Because 6 or 8 base toeholds are available for Inh to bind on $\alpha.T_1$ or $T_1.\alpha$, respectively, we took this toehold exchange reaction as fast as the binding of Inh to free T_1 (6 base toeholds have been shown to be sufficient to reach saturating hybridization speeds; Zhang and Winfree 2009),

- Parameters concerning two similar chemical processes, (for example polymerization of $\alpha.T_1$ versus that of $\alpha.T_2$, and more precisely for k^{α}_{pol}, k^{β}_{pol} and k^{Inh}_{pol}; for k^{α}_{pol} and $k^{\alpha}_{pol.SD}$; for k^{α}_{nick}, k^{β}_{nick} and k^{Inh}_{nick}; and for k^{Inh}_{a} and $k^{Inh}_{a.TH}$), were taken as identical.

The integration in these conditions gave the curve shown in Fig. 1D.

In order to avoid too much *a priori* considerations, these approximations were removed for the simulations during the optimization process, even when our biochemical measurement had shown very similar values for the parameters. The corresponding reactions and parameters constitute the 'optimized model'.

Synthesis of α:

$$T_1 + \alpha \underset{k_a^\alpha/K_a^\alpha}{\overset{k_a^\alpha}{\rightleftharpoons}} \alpha\cdot T_1$$
$$\alpha\cdot T_1 + \alpha \underset{k_a^\alpha/K_a^\alpha}{\overset{k_a^\alpha}{\rightleftharpoons}} \alpha\cdot T_1\cdot\alpha$$
$$T_1 + \alpha \underset{k_a^\alpha/K_a^\alpha}{\overset{k_a^\alpha}{\rightleftharpoons}} T_1\cdot\alpha$$
$$T_1\cdot\alpha + \alpha \underset{k_a^\alpha/K_a^\alpha}{\overset{k_a^\alpha}{\rightleftharpoons}} \alpha\cdot T_1\cdot\alpha$$
$$\alpha\cdot T_1 \xrightarrow{k_{pol}^\alpha} \alpha\alpha\cdot T_1$$
$$\alpha\cdot T_1\cdot\alpha \xrightarrow{k_{pol\cdot SD}^\alpha} \alpha\alpha\cdot T_1 + \alpha$$
$$\alpha\alpha\cdot T_1 \xrightarrow{k_{nick}^{T_1}} \alpha\cdot T_1\cdot\alpha$$

Synthesis of β:

$$T_2 + \alpha \underset{k_a^\alpha/K_a^\alpha}{\overset{k_a^\alpha}{\rightleftharpoons}} \alpha\cdot T_2$$
$$\alpha\cdot T_2 + \beta \underset{k_a^\beta/K_a^\beta}{\overset{k_a^\beta}{\rightleftharpoons}} \alpha\cdot T_2\cdot\beta$$
$$T_2 + \beta \underset{k_a^\beta/K_a^\beta}{\overset{k_a^\beta}{\rightleftharpoons}} T_2\cdot\beta$$
$$T_2\cdot\beta + \alpha \underset{k_a^\alpha/K_a^\alpha}{\overset{k_a^\alpha}{\rightleftharpoons}} \alpha\cdot T_2\cdot\beta$$
$$\alpha\cdot T_2 \xrightarrow{k_{pol}^\beta} \alpha\beta\cdot T_2$$
$$\alpha\cdot T_2\cdot\beta \xrightarrow{k_{pol\cdot SD}^\beta} \alpha\beta\cdot T_2 + \beta$$
$$\alpha\beta\cdot T_2 \xrightarrow{k_{nick}^{T_2}} \alpha\cdot T_2\cdot\beta$$

Synthesis of Inh:

$$T_3 + \beta \underset{k_a^\beta/K_a^\beta}{\overset{k_a^\beta}{\rightleftharpoons}} \beta\cdot T_3$$
$$\beta\cdot T_3 + Inh \underset{k_a^{Inh}/K_a^{Inh/T_3}}{\overset{k_a^{Inh}}{\rightleftharpoons}} \beta\cdot T_3\cdot Inh$$
$$T_3 + Inh \underset{k_a^{Inh}/K_a^{Inh/T_3}}{\overset{k_a^{Inh}}{\rightleftharpoons}} T_3\cdot Inh$$
$$T_3\cdot Inh + \beta \underset{k_a^\beta/K_a^\beta}{\overset{k_a^\beta}{\rightleftharpoons}} \beta\cdot T_3\cdot Inh$$
$$\beta\cdot T_3 \xrightarrow{k_{pol}^{Inh}} \beta Inh\cdot T_3$$
$$\beta\cdot T_3\cdot Inh \xrightarrow{k_{pol\cdot SD}^{Inh}} \beta Inh\cdot T_3 + Inh$$
$$\beta Inh\cdot T_3 \xrightarrow{k_{nick}^{T_3}} \beta\cdot T_3\cdot Inh$$

Inhibition:

$$T_1 + Inh \underset{k_a^{Inh}/K_a^{Inh/T_1}}{\overset{k_a^{Inh}}{\rightleftharpoons}} Inh\cdot T_1$$
$$T_1\cdot\alpha + Inh \underset{k_{a\cdot TH}^{Inh}K_a^\alpha/K_a^{Inh/T_1}}{\overset{k_{a\cdot TH}^{Inh}}{\rightleftharpoons}} Inh\cdot T_1 + \alpha$$
$$\alpha\cdot T_1 + Inh \underset{k_{a\cdot TH}^{Inh}K_a^\alpha/K_a^{Inh/T_1}}{\overset{k_{a\cdot TH}^{Inh}}{\rightleftharpoons}} Inh\cdot T_1 + \alpha$$

Exonuclease:

$$\alpha \xrightarrow{k_{exoN}^\alpha} \emptyset$$
$$\beta \xrightarrow{k_{exoN}^\beta} \emptyset$$
$$Inh \xrightarrow{k_{exoN}^{Inh}} \emptyset$$

Figure S9. Full reaction network of the Oligator system.

$$\frac{d[T_1]}{dt} = -k_a^{\alpha}[T_1][\alpha] + \frac{k_a^{\alpha}}{K_a^{\alpha}}[\alpha\cdot T_1] - k_a^{\alpha}[T_1][\alpha] + \frac{k_a^{\alpha}}{K_a^{\alpha}}[T_1\cdot\alpha] - k_a^{Inh}[T_1][Inh] + \frac{k_a^{Inh}}{K_a^{Inh/T_1}}[Inh\cdot T_1] \quad (1)$$

$$\frac{d[\alpha]}{dt} = -k_a^{\alpha}[T_1][\alpha] + \frac{k_a^{\alpha}}{K_a^{\alpha}}[\alpha\cdot T_1] - k_a^{\alpha}[\alpha][\alpha\cdot T_1] + \frac{k_a^{\alpha}}{K_a^{\alpha}}[\alpha\cdot T_1\cdot\alpha] - k_a^{\alpha}[T_1][\alpha] + \frac{k_a^{\alpha}}{K_a^{\alpha}}[T_1\cdot\alpha] - k_a^{\alpha}[\alpha][T_1\cdot\alpha] + \frac{k_a^{\alpha}}{K_a^{\alpha}}[\alpha\cdot T_1\cdot\alpha] \quad (2)$$
$$+ k_{pol\cdot SD}^{\alpha}[\alpha\cdot T_1\cdot\alpha] - k_a^{\alpha}[\alpha][T_2] + \frac{k_a^{\alpha}}{K_a^{\alpha}}[\alpha\cdot T_2] - k_a^{\alpha}[\alpha][T_2\cdot\beta] + \frac{k_a^{\alpha}}{K_a^{\alpha}}[\alpha\cdot T_2\cdot\beta] + k_{a\cdot TH}^{Inh}[T_1\cdot\alpha][Inh] - \frac{k_{a\cdot TH}^{Inh}\cdot K_a^{\alpha}}{K_a^{Inh/T_1}}[\alpha][Inh\cdot T_1]$$
$$+ k_{a\cdot TH}^{Inh}[\alpha\cdot T_1][Inh] - \frac{k_{a\cdot TH}^{Inh}\cdot K_a^{\alpha}}{K_a^{Inh/T_1}}[\alpha][Inh\cdot T_1] - k_{exoN}^{\alpha}[\alpha]$$

$$\frac{d[\alpha\cdot T_1]}{dt} = k_a^{\alpha}[T_1][\alpha] - \frac{k_a^{\alpha}}{K_a^{\alpha}}[\alpha\cdot T_1] - k_a^{\alpha}[\alpha][\alpha\cdot T_1] + \frac{k_a^{\alpha}}{K_a^{\alpha}}[\alpha\cdot T_1\cdot\alpha] - k_{pol}^{\alpha}[\alpha\cdot T_1] - k_{a\cdot TH}^{Inh}[\alpha\cdot T_1][Inh] + \frac{k_{a\cdot TH}^{Inh}\cdot K_a^{\alpha}}{K_a^{Inh/T_1}}[\alpha][Inh\cdot T_1] \quad (3)$$

$$\frac{d[\alpha\cdot T_1\cdot\alpha]}{dt} = k_a^{\alpha}[\alpha][\alpha\cdot T_1] - \frac{k_a^{\alpha}}{K_a^{\alpha}}[\alpha\cdot T_1\cdot\alpha] + k_a^{\alpha}[\alpha][T_1\cdot\alpha] - \frac{k_a^{\alpha}}{K_a^{\alpha}}[\alpha\cdot T_1\cdot\alpha] - k_{pol\cdot SD}^{\alpha}[\alpha\cdot T_1\cdot\alpha] + k_{nick}^{T_1}[\alpha\alpha\cdot T_1] \quad (4)$$

$$\frac{d[T_1\cdot\alpha]}{dt} = k_a^{\alpha}[T_1][\alpha] - \frac{k_a^{\alpha}}{K_a^{\alpha}}[T_1\cdot\alpha] - k_a^{\alpha}[\alpha][T_1\cdot\alpha] + \frac{k_a^{\alpha}}{K_a^{\alpha}}[\alpha\cdot T_1\cdot\alpha] - k_{a\cdot TH}^{Inh}[T_1\cdot\alpha][Inh] + \frac{k_{a\cdot TH}^{Inh}\cdot K_a^{\alpha}}{K_a^{Inh/T_1}}[\alpha][Inh\cdot T_1] \quad (5)$$

$$\frac{d[\alpha\alpha\cdot T_1]}{dt} = k_{pol}^{\alpha}[\alpha\cdot T_1] + k_{pol\cdot SD}^{\alpha}[\alpha\cdot T_1\cdot\alpha] - k_{nick}^{T_1}[\alpha\alpha\cdot T_1] \quad (6)$$

$$\frac{d[T_2]}{dt} = -k_a^{\alpha}[\alpha][T_2] + \frac{k_a^{\alpha}}{K_a^{\alpha}}[\alpha\cdot T_2] - k_a^{\beta}[T_2][\beta] + \frac{k_a^{\beta}}{K_a^{\beta}}[T_2\cdot\beta] \quad (7)$$

$$\frac{d[\alpha\cdot T_2]}{dt} = k_a^{\alpha}[\alpha][T_2] - \frac{k_a^{\alpha}}{K_a^{\alpha}}[\alpha\cdot T_2] - k_a^{\beta}[\alpha\cdot T_2][\beta] + \frac{k_a^{\beta}}{K_a^{\beta}}[\alpha\cdot T_2\cdot\beta] - k_{pol}^{\beta}[\alpha\cdot T_2] \quad (8)$$

$$\frac{d[\beta]}{dt} = -k_a^{\beta}[\alpha\cdot T_2][\beta] + \frac{k_a^{\beta}}{K_a^{\beta}}[\alpha\cdot T_2\cdot\beta] - k_a^{\beta}[T_2][\beta] + \frac{k_a^{\beta}}{K_a^{\beta}}[T_2\cdot\beta] + k_{pol\cdot SD}^{\beta}[\alpha\cdot T_2\cdot\beta] - k_a^{\beta}[\beta][T_3] + \frac{k_a^{\beta}}{K_a^{\beta}}[\beta\cdot T_3] \quad (9)$$
$$- k_a^{\beta}[\beta][T_3\cdot Inh] + \frac{k_a^{\beta}}{K_a^{\beta}}[\beta\cdot T_3\cdot Inh] - k_{exoN}^{\beta}[\beta]$$

$$\frac{d[\alpha\cdot T_2\cdot\beta]}{dt} = k_a^{\beta}[\alpha\cdot T_2][\beta] - \frac{k_a^{\beta}}{K_a^{\beta}}[\alpha\cdot T_2\cdot\beta] + k_a^{\alpha}[\alpha][T_2\cdot\beta] - \frac{k_a^{\alpha}}{K_a^{\alpha}}[\alpha\cdot T_2\cdot\beta] - k_{pol\cdot SD}^{\beta}[\alpha\cdot T_2\cdot\beta] + k_{nick}^{T_2}[\alpha\beta\cdot T_2] \quad (10)$$

$$\frac{d[T_2\cdot\beta]}{dt} = k_a^{\beta}[T_2][\beta] - \frac{k_a^{\beta}}{K_a^{\beta}}[T_2\cdot\beta] - k_a^{\alpha}[\alpha][T_2\cdot\beta] + \frac{k_a^{\alpha}}{K_a^{\alpha}}[\alpha\cdot T_2\cdot\beta] \quad (11)$$

$$\frac{d[\alpha\beta\cdot T_2]}{dt} = k_{pol}^{\beta}[\alpha\cdot T_2] + k_{pol\cdot SD}^{\beta}[\alpha\cdot T_2\cdot\beta] - k_{nick}^{T_2}[\alpha\beta\cdot T_2] \quad (12)$$

$$\frac{d[T_3]}{dt} = -k_a^{\beta}[\beta][T_3] + \frac{k_a^{\beta}}{K_a^{\beta}}[\beta\cdot T_3] - k_a^{Inh}[T_3][Inh] + \frac{k_a^{Inh}}{K_a^{Inh/T_3}}[T_3\cdot Inh] \quad (13)$$

$$\frac{d[\beta\cdot T_3]}{dt} = k_a^{\beta}[\beta][T_3] - \frac{k_a^{\beta}}{K_a^{\beta}}[\beta\cdot T_3] - k_a^{Inh}[\beta\cdot T_3][Inh] + \frac{k_a^{Inh}}{K_a^{Inh/T_3}}[\beta\cdot T_3\cdot Inh] - k_{pol}^{Inh}[\beta\cdot T_3] \quad (14)$$

$$\frac{d[Inh]}{dt} = -k_a^{Inh}[\beta\cdot T_3][Inh] + \frac{k_a^{Inh}}{K_a^{Inh/T_3}}[\beta\cdot T_3\cdot Inh] - k_a^{Inh}[T_3][Inh] + \frac{k_a^{Inh}}{K_a^{Inh/T_3}}[T_3\cdot Inh] + k_{pol\cdot SD}^{Inh}[\beta\cdot T_3\cdot Inh] - k_a^{Inh}[T_1][Inh] \quad (15)$$
$$+ \frac{k_a^{Inh}}{K_a^{Inh/T_1}}[Inh\cdot T_1] - k_{a\cdot TH}^{Inh}[T_1\cdot\alpha][Inh] + \frac{k_{a\cdot TH}^{Inh}\cdot K_a^{\alpha}}{K_a^{Inh/T_1}}[\alpha][Inh\cdot T_1] - k_{a\cdot TH}^{Inh}[\alpha\cdot T_1][Inh] + \frac{k_{a\cdot TH}^{Inh}\cdot K_a^{\alpha}}{K_a^{Inh/T_1}}[\alpha][Inh\cdot T_1] - k_{exoN}^{Inh}[Inh]$$

$$\frac{d[\beta\cdot T_3\cdot Inh]}{dt} = k_a^{Inh}[\beta\cdot T_3][Inh] - \frac{k_a^{Inh}}{K_a^{Inh/T_3}}[\beta\cdot T_3\cdot Inh] + k_a^{\beta}[\beta][T_3\cdot Inh] - \frac{k_a^{\beta}}{K_a^{\beta}}[\beta\cdot T_3\cdot Inh] - k_{pol\cdot SD}^{Inh}[\beta\cdot T_3\cdot Inh] + k_{nick}^{T_3}[\beta Inh\cdot T_3] \quad (16)$$

$$\frac{d[T_3\cdot Inh]}{dt} = k_a^{Inh}[T_3][Inh] - \frac{k_a^{Inh}}{K_a^{Inh/T_3}}[T_3\cdot Inh] - k_a^{\beta}[\beta][T_3\cdot Inh] + \frac{k_a^{\beta}}{K_a^{\beta}}[\beta\cdot T_3\cdot Inh] \quad (17)$$

$$\frac{d[\beta Inh\cdot T_3]}{dt} = k_{pol}^{Inh}[\beta\cdot T_3] + k_{pol\cdot SD}^{Inh}[\beta\cdot T_3\cdot Inh] - k_{nick}^{T_3}[\beta Inh\cdot T_3] \quad (18)$$

$$\frac{d[Inh\cdot T_1]}{dt} = k_a^{Inh}[T_1][Inh] - \frac{k_a^{Inh}}{K_a^{Inh/T_1}}[Inh\cdot T_1] + k_{a\cdot TH}^{Inh}[T_1\cdot\alpha][Inh] - \frac{k_{a\cdot TH}^{Inh}\cdot K_a^{\alpha}}{K_a^{Inh/T_1}}[\alpha][Inh\cdot T_1] + k_{a\cdot TH}^{Inh}[\alpha\cdot T_1][Inh] - \frac{k_{a\cdot TH}^{Inh}\cdot K_a^{\alpha}}{K_a^{Inh/T_1}}[\alpha][Inh\cdot T_1] \quad (19)$$

Figure S10. Full system of differential equation of the Oligator system.

Numerical Integration

The time evolution of this chemical network was computed by numerical integration of the set of ordinary differential equations. The simulation program was written in C, based on the GSL (http://www.gnu.org/software/gsl/) implementation of the implicit Bulirsch-Stoer algorithm (Bader and Deuflhard, 1983), and compiled using the GCC compiler v4.4. The computations were performed on a Dell Precision T5500 workstation, with a quadri-core Intel Xeon processor E5520, cadenced at 2.27 GHz, running an up-to-date Debian GNU/Linux

operating system. A typical single-processor integration process took about 200 ms to be performed.

The simulated time evolution could be quantitatively compared with the corresponding experimental measurement by computing the χ^2, using the formula:

$$\chi^2=\Sigma(x_{exp}-x_{sim})^2/(N\sigma)$$

The sum is done for each point of the curve, $(x_{exp}-x_{sim})$ being the difference between experimental and simulated values, and N the total number of points. σ is the standard deviation observed on the experimental data, and was evaluated for each curve. In the case of oligomer concentrations, the measurements were done in triplicate, so that the standard deviation could be calculated; the average value of these standard deviations was used for the calculation of χ^2. In the case of the fluorescence measurement, the noise was estimated by linear regression applied to a constant signal. A value of 1 for the χ^2 indicates a good estimation of the theoretical curve, lying within the error bars described by σ. Large values indicate the distance between the two curves.

Optimization Method

The process of parameter optimization was performed by a Python script, using the SciPy (http://www.scipy.org/) implementation of Powell's method (Press *et al*, 1992; Powell, 1964). It consisted in finding the set of normalized parameters p_{opt} that minimizes the function:

$$f(p_{opt})=w_1.\Sigma(p_{opt}-p_{exp})^2+w_2.\max(p_{opt}-p_{exp})+\chi^2(\alpha)+\chi^2(\beta)+\chi^2(Inh)+\chi^2(fluo)$$

$\Sigma(p_{opt}-p_{exp})^2$ indicates the distance between the tested set of parameters and the original set of parameters, $\max(p_{opt}-p_{exp})$ the maximum parameter drift, and the χ^2 the distance between the theoretical and experimental curves.

The fluorescence signal is supposed to be proportional to the number of base pairs plus a constant “background” value. However, the proportionality factor is not known, and was thus added as a parameter to be optimized. It was not used for the calculation of the constraints, so that it could be freely adjusted, with no cost.

The optimization process consists in performing different simulations for test sets of parameters p_{opt} and to evaluate the corresponding cost function $f(p_{opt})$. The space of parameter sets is scanned, starting from the experimental one, towards an optimal set that minimizes the cost function. Powell's algorithm drives the scanning process along an optimized route. These calculations result in parameters that can reproduce all the experimental inputs, while avoiding unrealistic drift of the parameters far away from their measured values. w_1 and w_2 are parameters that enable us to tune the weights for these constraints: low weights allow optimal curve fits, at the cost of larger parameter variations; high weights allow smaller parameter changes, at the cost of less accurate curve fits.

We conducted the optimization process with all experimental data of Fig. 2B and weights fixed at 2 and 20 for w_1 and w_2, resulting in very good adjustments ($\chi^2(\alpha) = 2.95$, $\chi^2(\beta) = 2.72$, $\chi^2(Inh) = 1.09$, $\chi^2(fluo) = 6.18$) while limiting the parameter drift to 15% on average, with a maximum of 28%. This optimization typically implied 50,000 evaluations of the cost function

(and thus the same number of simulations with different parameters) and took around 2-3 hours of single processor computation.

This optimized model offers a better understanding of the global functioning of the reaction network. As can be seen in Fig. S9 and S10, the system revolves on an orbit were most T_1 is always in the inhibited form. A very small concentration of uninhibited T_1 is sufficient to restart the autocatalytic accumulation of α and, even at its peak, active T_1 templates stay below approximately 2nM. Fig. S9 also shows that active T_2 templates oscillate on the same magnitude as active T_1 templates, but with a slight delay. This observation seems to corroborate the fact that total α and total β oscillations are experimentally measured with similar magnitudes, despite the difference in respective total templates concentrations.

Table SV: kinetic and thermodynamic parameters of the numerical optimization process

		Parameter name	Values used for numerical integration of the simple model[a]	Values obtained from optimization using the complete model	Relative drift from input value
Kinetic association constants ($10^6 M^{-1}min^{-1}$)		k_a^{α}	**26**	29	+12%
		k_a^{β}	**22**	17	-22%
		k_a^{Inh}	**30**	27	-10%
		$k_{a.TH}^{Inh}/k_a^{Inh}$	1	0.78	-22%
Thermo-dynamic association constants ($10^7 M^{-1}$)		K_a^{α}	**1.1**	0.86	-21%
		K_a^{β}	**2.7**	2.8	+4%
		K_a^{Inh/T_1}	**45**	44	-2%
		K_a^{Inh/T_3}	**120**	144	+20%
Enzymatic pseudo-first order rates (min^{-1})	*Bst* polymerase	k_{pol}^{α}	**17**	15	-12%
		$k_{pol}^{\beta}/k_{pol}^{\alpha}$	1	0.78	-22%
		$k_{pol}^{Inh}/k_{pol}^{\alpha}$	1	1.12	+12%
		$k_{pol.SD}^{\alpha}/k_{pol}^{\alpha} = k_{pol.SD}^{\beta}/k_{pol}^{\beta}$	1	0.78	-22%
		$k_{pol.SD}^{Inh}/k_{pol}^{Inh}$	**0.41**	0.33	-19%
	Nt.BstNBI nicking enzyme	$k_{nick}^{T_1}$	**3.0**	3.34	+11%
		$k_{nick}^{T_2}/k_{nick}^{T_1}$	1	0.78	-22%
		$k_{nick}^{T_3}/k_{nick}^{T_1}$	1	0.96	-4%
	$RecJ_f$ exonuclease	k_{exoN}^{α}	**0.32**	0.41	28%
		$k_{exoN}^{\beta}/k_{exoN}^{\alpha}$	**1.16**	1.18	2%
		$k_{exoN}^{Inh}/k_{exoN}^{\alpha}$	**3.75**	4.2	12%
Initial conditions (10^{-9}M)		T_1	**30**	38	+27%
		T_2	**5**	3.9	-22%
		T_3	**30**	38	+27%

[a] values in bold are experimental values.

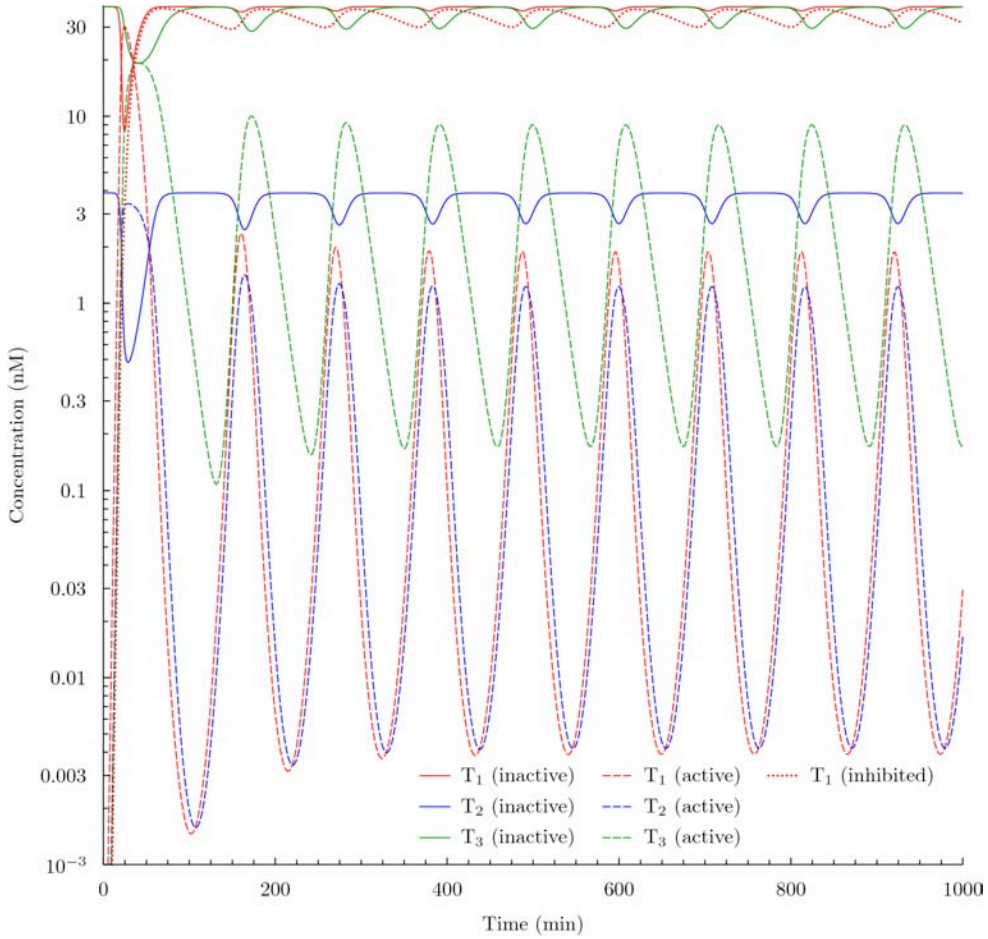

Figure S11. Analysis of the 'optimized model'. The plot shows the calculated evolution of the three templates, classified as 'active' (currently producing their output, ie $\alpha.T_1+\alpha.T_1.\alpha+\alpha\alpha.T_1$; $\beta.T_2+\alpha.T_2.\beta+\alpha\beta.T_2$; $\beta.T_3+\beta.T_3.Inh+\beta Inh.T_3$) or 'inactive' (not producing or inhibited, ie $T_1+Inh.T_1+T_1.\alpha$; $T_2+T_2.\beta$; $T_3+T_3.Inh$). We also plot the evolution of $Inh.T_1$ to emphasize the fact that a large fraction of T_1 templates is always in this inhibited form.

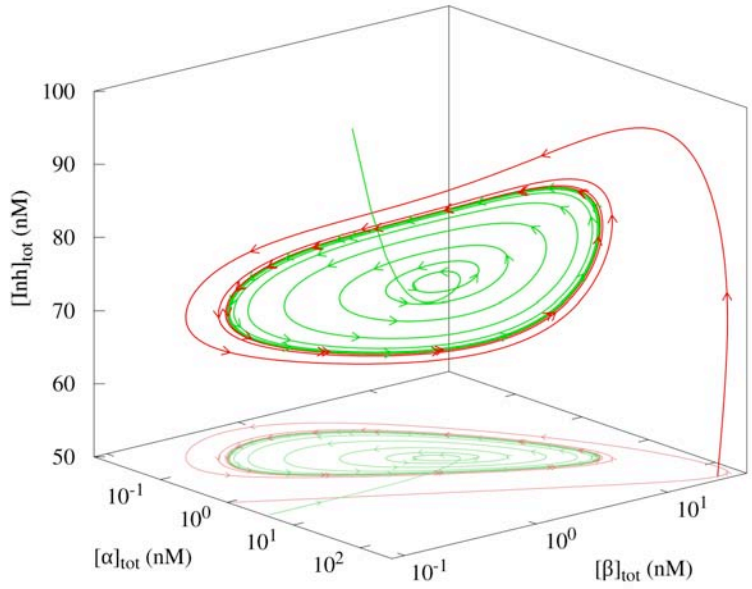

Figure S12. Phase trajectory of the 'optimized model'. The trajectories are presented for 2 different initial conditions. The red trajectory corresponds to the initial condition of Fig 1C and 2 in the main text, showing oscillations of decreasing amplitude until they reach the limit cycle. The green trajectory corresponds to a system starting close to an unstable focus point, showing oscillations of increasing amplitude until they reach the limit cycle. This type of behavior is typical of a Hopf bifurcation (Epstein and Pojman 1998).

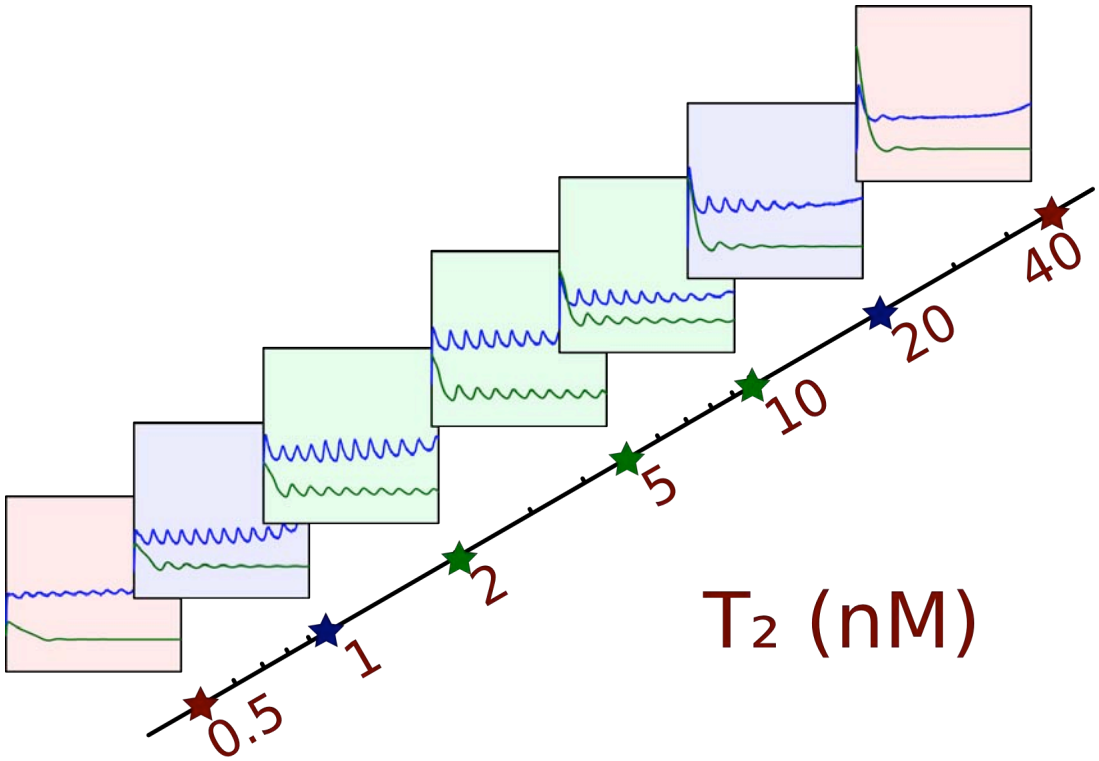

Figure S13. Behaviour of the Oscillator along the [T2] axis and comparison with model predictions. Each frame shows the fluorescence (a.u.) from t = 0 to 1000 minutes, at [T1]=30nM, [T3]=30nM and [T2] corresponding to the position of the corresponding star on the axis. Blue line: experiments; green line: predictions made with the set of parameters of the 'optimized model'. Green, blue and red frames correspond to sustained, damped or non-oscillating experiments, respectively.

Supplementary References

Bader G, Deuflhard PA (1983) semi-implicit mid-point rule for stiff systems of ordinary differential equations, *Numer Math* **41:** 373

Han ES, Cooper DL, Persky NS, Sutera VA, Whitaker RD, Montello ML, Lovett ST (2006) RecJ exonuclease: substrates, products and interaction with SSB. *Nucl Acids Res* **34:** 1084-1091

Kong HM, Kucera RB, Jack WE (1993) Characterization of a DNA Polymerase from the Hyperthermophile Archaea Thermococcus litoralis. *J Biol Chem* **268:** 1965

Kramer MF, Coen DM (2001) Enzymatic Amplification of DNA by PCR: *Standard Procedures and Optimization Current Protocols in Molecular Biology* 15.1.1

Lovett ST, Kolodner RD (1989) Identification and purification of a single-stranded-DNA-specific exonuclease encoded by the recJ gene of Escherichia coli. *Proc Natl Acad Sci USA* **86:** 2627

Markham NR, Zuker M (2005) DINAMelt web server for nucleic acid melting prediction. *Nuc Acids Res* **33:** 577

Mao F, Leung W-Y, Xin X (2007) Characterization of EvaGreen and the implication of its physicochemical properties for qPCR applications. *BMC Biotechnology* **7:**76

Mergny JL, Lacroix L (2002) Des Tms encore des Tms, toujours des Tms, *Regards/biochimie* **2**: 36

Nelson JW, Tinoco IJ (1982) Comparison of the kinetics of ribooligonucleotide, deoxyribooligonucleotide, and hybrid oligonucleotide double-strand formation by temperature jump kinetics. *Biochemistry* **21**, 5289

Powell MJ (1964) An efficient method for finding the minimum of a function of several variables without calculating derivatives, *Comp J* **7:** 152

Press WH, Flannery BP, Teukolsky SA, Vettering WT (1992) Numerical recipes in C: the art of scientific computing. 2nd ed. Cambridge University Press: Cambridge, 724-731 & 412-419

Riggs MG, Tudor S, Sivaram M, McDonough SH (1996) Construction of single amino acid substitution mutants of cloned Bacillus stearothermophilus DNA polymerase I which lack 5' 3'exonuclease activity. *Biochim Biophys Acta* **1307**: 178

Spiess AJ, Mueller N, Ivell R (2004) Trehalose Is a Potent PCR Enhancer: Lowering of DNA Melting Temperature and Thermal Stabilization of Taq Polymerase by the Disaccharide Trehalose. *Clin Chem* **50:** 1256

Stein CA, Subasinghe C, Shinozuka K, Cohen JS (1988) Physicochemical properties of phosphorothioate oligodeoxynucleotides. *Nucl Acids Res* **16:** 3209-3221

Tan E, Erwin B, Dames S, Ferguson T, Buechel M, Irvine B, Voelkerding K, Niemz A (2008) Specific versus Nonspecific Isothermal DNA Amplification through Thermophilic Polymerase and Nicking Enzyme Activities. *Biochemistry* **47**: 9987

Van Ness J, Van Ness LK, Galas DJ (2003) Isothermal reactions for the amplification of

oligonucleotides. *Proc Natl Acad Sci USA* **100:** 4504